

Exciton/biexciton energies in rectangular GaAs/Al_xGa_{1-x}As quantum-well wires including finite Al-graded band offsets with application to third-order optical susceptibilities

Frank L. Madarasz

Optical Science and Engineering Program and Center for Applied Optics, University of Alabama in Huntsville, Huntsville, Alabama 35899

Frank Szmulowicz and F. Kenneth Hopkins

Wright Laboratory, Materials Directorate (WL/MLPO), Wright-Patterson Air Force Base, Dayton, Ohio 45433-7707

(Received 21 February 1995; revised manuscript received 13 April 1995)

Exciton and biexciton binding energies and wave functions are calculated with a three-parameter variational model in an effective-mass approximation for a rectangular GaAs quantum-well wire surrounded by an Al_xGa_{1-x}As cladding. Moreover, the Al interdiffusion into the wire and the finite band offsets between the wire and the cladding have been included. For the range of dimensions studied, the inclusion of the Al interdiffusion had a pronounced effect on the binding energies when compared to those obtained from the infinite barrier model [Frank L. Madarasz, Frank Szmulowicz, F. Kenneth Hopkins, and Donald L. Dorsey, *Phys. Rev. B* **49**, 13 528 (1994); *J. Appl. Phys.* **75**, 639 (1994); *Phys. Rev B* **51**, 4633 (1995)]. Using the results of the exciton and biexciton calculation, we calculate the third-order nonlinear optical susceptibility as a function of pump-probe frequencies in a small range about the exciton absorption resonance. We have found, depending upon wire dimensions, broadening parameter(s) size, and the amount of pump detuning, values of the imaginary parts of the susceptibilities to be on the order of -10^{-1} esu and a fairly large off-resonance absorption due to biexciton formation.

I. INTRODUCTION

Excitonic properties have been extensively modeled in quantum wells, wires, and dots.¹⁻¹⁹ For the lowest-dimensional confinement of a quantum well, it is possible to construct analytically a model which incorporates accurately the physics and the geometry:^{11,12} finite barrier potentials and band offsets, barrier penetration, parabolic shaped wells, etc. Rectangular quantum-well wires (QWW's), on the other hand, are more difficult. In general, because of two-dimensional confinement, the Hamiltonian is not precisely separable unless the two orthogonal potentials are infinite.^{1,2,13,14} Because of this problem, most exciton structure modeling has been done for the ideal case of cylindrical wires with an infinite potential at the circumference of the wire. When considering the biexciton binding energy—which is needed for the calculation of $\chi^{(3)}$ —an effective one-dimensional Coulomb potential in the radial direction was employed;⁵ still, $\chi^{(3)}$ was not explicitly calculated. In a subsequent publication,²⁰ Bányai *et al.*, the authors of Ref. 5, extended that work to the calculation of the total absorption coefficient and total refractive index (both related to the total χ) for various beam intensities in a two-photon absorption model. On the other hand, Glutsch and Bechstedt¹ have approximated the separation of the two-dimensional potential in orthogonal directions in a square wire with the condition that the potential in one direction is infinite while in the other direction is finite. Their interest, though, was only in calculating the spatially non-local absorption $\chi^{(1)}$ by single excitons; no attempt was made to determine $\chi^{(3)}$.

Madarasz and co-workers¹⁴⁻¹⁶ have calculated exciton and biexciton binding energies and wave functions in rec-

tangular GaAs wires, and have applied the results to the problem of $\chi^{(3)}$ for a pump-probe experiment. The calculation was done variationally utilizing three variational parameters. The Coulomb interaction terms were treated exactly in their full three-dimensional form throughout the calculation, especially in the case of the biexciton, which is a more physically realistic procedure than employed in previous calculations that relied upon an effective one-dimensional potential(s). As a result, if one dimension of the rectangular wire is nonzero, no matter how small, the other may be collapsed to zero without giving rise to an infinite energy. A unique feature of the calculation was its use of a two-dimensional Fourier expansion of the Coulomb potential(s), which removes the numerical difficulty with the $1/r$ singularity, and considerably reduces the computational effort. The results of the excitonic electronic structure computation were then applied to the problem of the third-order nonlinear optical susceptibility. With the goal of determining peak values of susceptibilities for various cross-sectional wire dimensions, $\chi^{(3)}$ was first expanded in the density-matrix formalism, and then evaluated for near-resonant exciton absorption in the rotating-wave approximation (RWA).²¹ Values of $|\text{Im}\chi^{(3)}|$ on the order of 10^{-1} esu were obtained.

High quality rectangular QWW's have most recently been manufactured via Al-Ga interdiffusion from the cladding material due to local heating by means of a focused laser.²² A similar technique is being pursued using focused ion-beam technology.²³ In both cases, the potentials in the lateral directions are graded due to the Al interdiffusion. The previous model by Madarasz and co-workers¹⁴⁻¹⁶ assumes an abrupt infinite potential in the lateral direction. In the present paper we refine and ex-

tend that model to include finite graded barrier potentials for the electrons and holes in the lateral direction. In Sec. II A, we review the original exciton/biexciton theory, making the necessary changes to include the Al interdiffusion. In Sec. II B we display the expression of the third-order optical susceptibility, now including terms beyond the RWA. Results and discussion are given in Sec. III. Finally, a summary is given in Sec. IV.

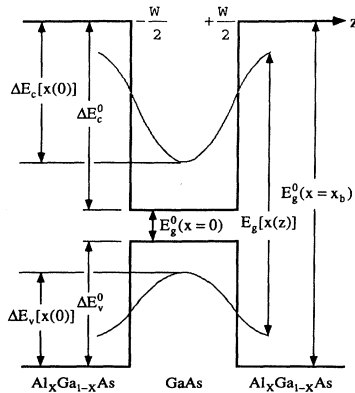
II. THEORY

In the present work we build upon the existing infinite potential barrier model of Madarasz and co-workers.^{14–16} The reader is referred to our original papers for the complete and quantitative details of our basic model. Here we will outline the basic theory including the appropriate modifications needed to incorporate the Al interdiffusion into the wire from the surrounding cladding material.

A. Excitonic properties

The interdiffusion is in the lateral direction, here taken as the z direction. Since the potential in the orthogonal direction is square and we are interested only in the lowest-lying states, we may approximate it, relative to the lateral direction, as infinite. Figure 1 defines the quantities needed in order to calculate the electron and hole potential energies V_e and V_h , respectively. The finite conduction ΔE_c^0 and valence ΔE_v^0 band offsets are taken to be in the ratio of 60/40. All quantities are graded with the interdiffusion Al composition distribution $x(z)$. Following the work of Madarasz and Szmulowicz²⁴ on Cd interdiffusion across $\text{Hg}_x\text{Cd}_{1-x}\text{Te}$ heterojunctions, the Al grading distribution will be taken as

Finite Potential Well and Aluminum Interdiffusion



$$V_e(z) = 0.6 [E_g[x(z)] - E_g[x(0)] + E_g^0(x=0)]$$

$$V_h(z) = -0.4 [E_g[x(z)] - E_g[x(0)]]$$

FIG. 1. Definition of quantities used in the calculation of the finite Al-graded band-offset potential energies.

$$x(z) = x_0 + x_c + \left[\frac{x_c - x_0}{2} \right] \left\{ \operatorname{erf} \left[\frac{z - z_0^+}{C} \right] - \operatorname{erf} \left[\frac{z - z_0^-}{C} \right] \right\}, \quad (1)$$

where x_0 (here zero) and x_c are the Al compositions in the wire and cladding material, respectively, $z_0^\pm = \pm W/2$, and $2C$ is the Al grading width in which the Al composition changes by 85%.

The Schrödinger equation for single-particle states in the lateral direction is

$$-\frac{\hbar^2}{2} \frac{d}{dz} \left\{ \frac{1}{m_i^*[x(z)]} \frac{du_i^{(n)}(z)}{dz} \right\} + V_i[x(z)] u_i^{(n)}(z) = E_i^{(n)} u_i^{(n)}(z), \quad i=e, h, \quad n=1, 2, 3, \dots, \quad (2)$$

where $E_i^{(n)}$ is the eigenenergy of the n th subband. Equation (2) must be solved numerically. This we did with a modified fourth-order Runge-Kutta routine which accounts for the values of the variable coefficients $m_i^*[x(z)]$ and $V_i[x(z)]$ between the node points of the integration mesh. Here m_i^* and V_i are written as functions of $x(z)$ to emphasize their implicit dependence on the Al compositional grading; $x(z)$ should not be confused with the coordinate x .

In the envelope-function approximation (EFA), the exciton Hamiltonian is given by

$$H_{\text{ex}} = \frac{p_{ye}^2}{2m_c^*} + \frac{p_{yh}^2}{2m_\perp^*} + \frac{p_x^2}{2\mu} - \frac{e^2}{\epsilon\sqrt{x^2 + \rho^2}} + E_g^0 + V_e(z) + V_h(z), \quad (3)$$

where m_c^* is the electron conduction-band effective mass, m_\perp^* is the heavy-hole valence-band effective mass perpendicular to the axis of the wire, μ is the heavy-hole exciton reduced mass, e is the charge of an electron, ϵ is the static dielectric constant, E_g^0 is the fundamental band gap of the wire material, and $\rho^2 = (y_e - y_h)^2 + (z_e - z_h)^2$ is the exciton cylindrical radius in the confined directions.

Even for this relatively simple Hamiltonian no exact solution is possible. The envelope function is then chosen to be a trial wave function in a variational procedure:

$$\psi = \frac{2}{L} g_t(x; \eta_x) \cos(k_y y_e) \cos(k_y y_h) u_e^{(1)}(z_e) u_h^{(1)}(z_h), \quad (4)$$

where $g_t(x; \eta_x)$ is a Gaussian-type orbital function,

$$g_t(x; \eta_x) = \frac{1}{\sqrt{\eta_x}} \left[\frac{2}{\pi} \right]^{1/4} \exp \left[-\frac{x^2}{\eta_x^2} \right], \quad (5)$$

in which η_x is the e - h variational parameter, and $k_y = \pi/L$.

The variational parameter η_x is determined by minimizing the expectation value of the exciton Hamiltonian with respect to η_x ; its value will reflect the dimensions of the wire and specific values of the material parameters

used. The only components of the Hamiltonian which depend on η_x are the kinetic energy of the relative motion, and the e - h interaction term. Together, they define the exciton binding energy:¹⁵

$$E_{K\mu}^x = \left\langle \psi \left| \frac{p_x^2}{2\mu} \right| \psi \right\rangle = \frac{\hbar^2}{2\mu} \frac{1}{\eta_x^2} \quad (6)$$

and

$$V_{eh} = V(|x\mathbf{i} + \rho_e - \rho_h|) = \left\langle \psi \left| \frac{(-)e^2}{\epsilon\sqrt{x^2 + \rho^2}} \right| \psi \right\rangle \quad (7a)$$

$$= (-) \frac{e^2}{2\pi} \frac{1}{\eta_x} \int_0^{2\pi} d\phi \times \int_0^{+\infty} dQ_{\eta_x} I(Q_{\eta_x}) H_{LW}(Q_{\eta_x}, \phi) . \quad (7b)$$

The integrand is given by

$$I(Q_{\eta_x}) = \exp(Q_{\eta_x}/2\sqrt{2})^2 [1 - \operatorname{erf}(Q_{\eta_x}/2\sqrt{2})] , \quad (8)$$

where erf is an error function. The factor $H_{LW} = H_L H_W$, where

$$H_L(Q_{\eta_x}, \phi) = \frac{\pi^4}{\left[\pi^2 - \left[\frac{L}{2\eta_x} Q_{\eta_x} \sin\phi \right]^2 \right]^2} \times \frac{\sin^2 \left[\frac{L}{2\eta_x} Q_{\eta_x} \sin\phi \right]}{\left[\frac{L}{2\eta_x} Q_{\eta_x} \sin\phi \right]^2} \quad (9a)$$

and

$$H_W(Q_{\eta_x}, \phi) = \int_{-\infty}^{+\infty} dz_e \exp \left[-i \frac{Q_{\eta_x}}{\eta_x} \cos\phi z_e \right] |u_e^{(1)}(z_e)|^2 \times \int_{-\infty}^{+\infty} dz_h \exp \left[-i \frac{Q_{\eta_x}}{\eta_x} \cos\phi z_h \right] |u_h^{(1)}(z_h)|^2 . \quad (9b)$$

The biexciton Hamiltonian is considerably more complicated, since it involves the interaction of four particles. The kinetic-energy operator is

$$E_K^{xx} = -\frac{\hbar^2}{2\mu} \left[\frac{\partial^2}{\partial x_{1a}^2} + \frac{\partial^2}{\partial x_{2b}^2} \right] - \frac{\hbar^2}{m_{\parallel}^*} \left[\frac{\partial}{\partial x_{ba}} + \frac{\partial}{\partial x_{1a}} - \frac{\partial}{\partial x_{2b}} \right] \frac{\partial}{\partial x_{ba}} - \frac{\hbar^2}{2m_c^*} \left[\frac{\partial^2}{\partial y_1^2} + \frac{\partial^2}{\partial y_2^2} \right] - \frac{\hbar^2}{2m_{\perp}^*} \left[\frac{\partial^2}{\partial y_a^2} + \frac{\partial^2}{\partial y_b^2} \right] - \frac{\hbar^2}{2} \frac{\partial}{\partial z} \left[\frac{1}{m_c^*(z)} \frac{\partial}{\partial z} \right] - \frac{\hbar^2}{2} \frac{\partial}{\partial z} \left[\frac{1}{m_{\perp}^*(z)} \frac{\partial}{\partial z} \right] , \quad (10)$$

where m_{\parallel}^* is the effective mass parallel to the wire axis, and the potential energy is

$$V_{xx} = \frac{e^2}{\epsilon} \left[\frac{(-)1}{\sqrt{x_{1a}^2 + \rho_{1a}^2}} + \frac{(-)1}{\sqrt{x_{2b}^2 + \rho_{2b}^2}} + \frac{(-)1}{\sqrt{x_{2a}^2 + \rho_{2a}^2}} + \frac{(-)1}{\sqrt{x_{1b}^2 + \rho_{1b}^2}} + \frac{(+1)}{\sqrt{x_{ba}^2 + \rho_{ba}^2}} + \frac{(+1)}{\sqrt{x_{21}^2 + \rho_{21}^2}} \right] , \quad (11)$$

where 1 and 2 label the electron coordinates, and a and b label the hole coordinates, $x_{\alpha\beta} = x_{\alpha} - x_{\beta}$, $\rho_{\alpha\beta} = (y_{\alpha} - y_{\beta})\mathbf{j} + (z_{\alpha} - z_{\beta})\mathbf{k}$, and $\alpha, \beta = 1, 2, a$, or b .

Since it is not possible to solve a four-body problem exactly, again a variational approach is employed. The trial wave function includes the Heitler-London approximation for the e - h pair contributions and is of the form¹⁵

$$\Psi = \frac{1}{S(x_{ba})} [\psi_{1a}\psi_{2b} + \psi_{2a}\psi_{1b}] \psi_{ba} . \quad (12)$$

$\psi_{\alpha\beta}$ is of the general form of Eq. (4) but with $g_i(x; \eta_x) = g_{\alpha\beta}(x_{\alpha\beta}; \eta_{xx})$ given by Eq. (5), but not normalized, where η_{xx} is the e - h variational parameter within the excitonic molecule, and $g_{ba} = g_{ba}(x_{ba}; \xi)$, which is normalized, is a function of the hole-hole variational parameter ξ . $S(x_{ba})$ is the normalization factor.

The final expressions for the expectation values of both the kinetic and potential energies are long and complicated. They may be found in their entirety in the paper by Madarasz *et al.*¹⁵ What is important for the present work is just their functional forms, which are represented by \mathcal{H} and \mathcal{P} . The kinetic energy and potential energies are

$$E_K^{xx} = 2E_K^x + \mathcal{H}(\eta_{xx}; \xi) , \quad (13)$$

where E_K^x is the total kinetic energy of a single exciton, and

$$V_{xx} = \frac{e^2}{2\pi\epsilon} \frac{1}{\eta_{xx}} \int_0^{+\infty} dQ_{\eta_{xx}} \int_0^{2\pi} d\phi \{ \mathcal{P}[I_1^{(ba)}, I_1^{(1a)}, I_2^{(1a)}, I_3^{(1a)}; I_0^{(21)}, I_1^{(21)}, I_2^{(21)}] H_{LW}(Q_{\eta_{xx}}, \phi) \}, \quad (14)$$

where the I 's are functions of $Q_{\eta_{xx}}$, η_{xx} , and ξ , and each is made up of two terms similar in form to Eq. (8). $H_{LW}(Q_{\eta_{xx}}, \phi)$ is identical to Eq. (9), but with $\eta_x = \eta_{xx}$. As in the case of the single exciton, the biexciton Hamiltonian must be minimized with respect to the variational parameters in order to obtain the biexciton binding energy.

Since the biexciton wave function of Eq. (12) is made up of single-particle states—now given by Eq. (4)—the Al-graded potential will also affect the biexciton binding energy.

B. Nonlinear optical properties

Pump-probe spectroscopy is used experimentally to extract excitonic optical nonlinearities from other nonlinearities in semiconducting materials. We restrict our

calculation to the optical nonlinearity via the biexciton state arising from the population saturation of the exciton state. For resonant excitation, the expression for $\chi^{(3)}$ in the RWA (Ref. 20) is given by Refs. 14–16. However, here we wish to investigate the frequency dependence of $\chi^{(3)}$ in a narrow range about the resonant exciton absorption line. The general derivation of $\chi^{(3)}$ for low-density exciton/biexciton systems is given in the Appendix of our previous paper;¹⁵ it is based on the summation over 16 double Feynman diagrams.^{21,25} The spurious size dependence which generally accompanies the derivation of $\chi^{(3)}$ for a local two-level system has been eliminated by taking into account the Pauli exclusion principle; that is, one physical site is not allowed to be doubly excited.^{21,25}

In the frequency range of interest, the lowest-lying states are the major contributors to $\chi^{(3)}$. Accordingly, the general expression reduces to

$$\begin{aligned} \chi^{(3)} = & \frac{(-)2}{\pi\sqrt{2\pi}} \left[\frac{n_0}{\eta_x} \right] \left[\frac{\xi}{\eta_x} \right] \frac{e^4}{m_0^2 \omega_{g0}^4} E_p^2 \left[\frac{1}{(\omega_1 - \omega_{g0} + i\Gamma_{g0})} - \frac{1}{[\omega_1 - \omega_{g0} + \omega_{bx}(\eta_{xx}, \xi) + i\Gamma_{bg}]} \right] \\ & \times \left[\sum_{r=1}^2 \left\{ \frac{1}{\hbar^3(\omega_r - \omega_2 + i\gamma)} \left(\frac{1}{(\omega_{g0} - \omega_2 + i\Gamma_{g0})} + \frac{1}{(\omega_r - \omega_{g0} + i\Gamma_{g0})} \right) \right\} \right. \\ & \left. + \frac{1}{(\omega_1 + \omega_2 - 2\omega_{g0} + \omega_{bx}(\eta_{xx}, \xi) + i\Gamma_{b0})} \left(\frac{1}{(\omega_1 - \omega_{g0} + i\Gamma_{g0})} + \frac{1}{(\omega_2 - \omega_{g0} + i\Gamma_{g0})} \right) \right], \quad (15) \end{aligned}$$

where ω_2 and ω_1 are the pump-probe frequencies, respectively, n_0 is the average areal density of unit cells, m_0 is the rest mass of an electron, e is the charge on an electron, E_p is the Kane matrix element and $\hbar\omega_{bx}$ is the biexciton binding energy. γ and Γ_{ij} are longitudinal and transverse relaxation/broadening parameters, respectively. The ij indices refer to the o -system ground state, g -exciton ground state; and b -biexciton ground state. $1/\gamma = 1/\Gamma_{ii}$ is the population decay time for state i , and $1/\Gamma_{ij}$ is the dephasing or lifetime of the coherent superpositions between states i and j . Note that, if all transverse relaxation parameters are assumed to be equal, the model reduces to the independent boson model. Then, when the biexciton binding energy approaches zero so does the third-order susceptibility, because of the first bracketed factor in Eq. (15), as it should.

III. RESULTS AND DISCUSSION

In order to calculate the exciton and biexciton binding and ground-state energies and optical susceptibilities, we employed the physical parameters summarized in Table I. All parameters needed but not listed in Table I are shown in the figures.

The Al interdiffusion in the lateral direction requires a numerical solution to Eq. (2) for the single-particle elec-

tron and hole states. As a part of this numerical approach one must search for the integration range, i.e., numerical infinity, in which the wave function appropriately tends to zero and yields the correct corresponding eigenvalue: this must be done for every set of cross-sectional dimensions and for each characteristic Al-grading width $2C$. In turn, the values of the three variational parameters are changed; one must further search for an acceptable starting value of the exciton variational parameter in order to start the minimization process. Needless to say, the whole process is time consuming. Thus, for illustrative purposes, we have limited ourselves to one set of wire dimensions— $L \times W = 125 \times 75 \text{ \AA}^2$ —and four characteristic diffusion lengths— $C = W/16, W/8, W/4,$ and $W/2$. This particular set of wire dimensions was chosen because it is on the order of the bulk exciton radius and

TABLE I. Physical parameters for $\text{Al}_x\text{Ga}_{1-x}\text{As}$.

$x =$	0.0	0.3
$E_g^0 =$	1.512 eV ^a	1.899 eV ^a
$m_{\perp}^* =$	0.450 m_0	0.576 m_0
$m_e =$	0.067 m_0	0.092 m_0
$m_{\parallel}^* = 0.027m_0$ (Refs. 4 and 14)		$\epsilon = 12.5$
$n_0 = 7.89 \times 10^{14}/\text{cm}^2$	$E_p = 23.0 \text{ eV}$	

^a $E_g^0(x) = 1.512 + 1.155x + 0.37x^2$.

corresponds to a peak third-order optical susceptibility calculated for the infinite barrier model. The results of the electronic part of the calculation are summarized in Table II.

With reference to Table II, we first note that the inclusion of finite band offsets lowers both electron and hole single-particle subband energies for the narrowest grading (almost abruptly), $W/16$, giving approximately a 61% difference for the electron and a 35% difference for the hole. Of course this is precisely what is expected to happen. Fixing our attention on just the electron states for the moment, we see that, by increasing the diffusion length from $W/16$ to $W/8$ and then from $W/8$ to $W/4$, the subband energies rise. The reason for this trend is clear especially when we consider the graded well structure plotted in Fig. 1: as the diffusion width is increased the bottom of the well narrows, pushing the states up. However, when increasing the diffusion length from $W/4$ to $W/2$ the trend appears to be reversed. The cause of this reversal is also clear: the well is now "overgraded." That is, under this condition, there is enough Al concentration located at the center of the well to change the fundamental gap from that of pure GaAs to some percentage of $\text{Al}_x\text{Ga}_{1-x}\text{As}$ —the gap is increased and the well, as it rises, begins to flatten out. Relative to the bottom of the graded well the subband energy has indeed become smaller, but relative to the bottom of the GaAs well it has continued to rise. In fact, as the fraction of Al in the center of the graded well approaches $x=0.3$, the subband(s) coalesces at the bottom of the well and forms the conduction band in bulk $\text{Al}_x\text{Ga}_{1-x}\text{As}$; the lowering of subband energies is to be expected.

A similar argument can be made for the hole subband energies. However, it is apparent from Table II that, when the diffusion length reaches $W/4$, the subband energy exceeds that of the infinite barrier model. The cause of such a result is not totally unexpected. The barrier height for the holes is two-thirds of that for the electrons.

TABLE II. Infinite versus finite potential barrier results. $L \times W = 125 \times 75\text{-}\text{\AA}^2$ GaAs wire/ $\text{Al}_{0.3}\text{Ga}_{0.7}\text{As}$ cladding^a.

	Infinite	$W/16^b$	$W/8^b$	$W/4^b$	$W/2^b$
ϵ_1^e (meV)	99.75	38.67	41.69	51.38	47.24
ϵ_1^h (meV)	14.85	9.66	11.11	16.73	16.76
η_x (a_0)	362.20	395.45	393.58	389.95	395.12
E_B^x (meV)	-14.23	-12.27	-12.35	-12.54	-12.29
V_{eh} (meV)	-19.69	-16.85	-16.97	-17.25	-16.88
E_{g0}^x (eV)	1.662	1.597	1.602	1.617	1.668
$\xi(a_0)$	1024.43	1116.79	1111.62	1101.55	1115.88
$\eta_{xx}(a_0)$	293.38	320.36	318.86	313.96	318.09
E_B^{xx} (meV)	-9.71	-8.36	-8.42	-8.55	-8.38
V^{xx} (meV)	-53.61	-45.88	-46.22	-46.97	-45.97
E_{g0}^{xx} (eV)	3.31	3.186	3.195	3.225	3.328
$z(0.01u_{e\max}^{(1)})$ (\AA)		97.00	99.00	100.00	115.00
$z(0.01u_{h\max}^{(1)})$ (\AA)		61.00	62.00	63.00	69.00

^aBand offsets—0.6 conduction, 0.4 valence.

^b $\frac{1}{2}$ Al grading width.

This means that the corresponding Al grading of the valence band produces a well which is narrower for $z < W/2$ and wider for $z > W/2$ than that of the conduction band. One then expects a larger percentage increase in energy for the lower-lying hole subband bands. For example, changing the diffusion length from $W/8$ to $W/4$ produces about a 19% increase in the electron subband energy, and about a 34% increase in the hole subband energy.

The exciton and biexciton binding energies are lowered with the inclusion of the finite band offsets by approximately 14% for the smallest diffusion length of $W/16$. The evolution of their respective values with increasing Al grading width can easily be explained in terms of the arguments given above for the electron and hole subbands. Similarly, the exciton and biexciton ground-state energies are lowered with the inclusion of the finite band offsets. Since each is dominated by the fundamental band-gap energy, their change is rather small, both being approximately 4% for the smallest diffusion length of $W/16$. Because of such a small change in the exciton ground-state energy, the effect on the magnitude of the optical susceptibility is negligible. However, at higher densities of excitons and biexcitons than considered here, the lower binding energies do affect the stability of the system and will thus limit the operational conditions under which peak $\chi^{(3)}$ values may be obtained and maintained.

The structure in $\chi^{(3)}$ is a strong function of the values of the longitudinal and transverse relaxation parameters. These parameters are quite difficult to obtain accurately by experiment, and there are no first-principles theoretical models of which we are aware. In addition, they are probably strong functions of the confinement dimensions as well as the population density of the excitons and temperature.^{26,27} Consequently, some researchers have chosen them to be equal—for example, Refs. 18 and 19—while some have used them as fitting parameters—for example, Refs. 17 and 19. There is, however, good reason to believe that the longitudinal parameter is perhaps as much as an order of magnitude smaller than the transverse parameters.^{17,20} Accordingly, for comparison, we have calculated $\chi^{(3)}$ for values $\gamma=0.1\Gamma_0$ and all $\Gamma_{ij}=\Gamma_0$, and for $\gamma=\Gamma_{ij}=\Gamma_0$, where $\sqrt{2}\Gamma_0$ corresponds to the full width at half maximum (FWHM) of the Gaussian representing the exciton linear absorption.

In Figs. 2–7 we have calculated $\text{Im}\chi^{(3)}$ for a two-beam experiment in which one beam, the pump, is fixed and the other, the probe, is allowed to vary over a frequency range in which the pump is fixed. Specifically, in Figs. 2 and 3 the pump is fixed right on the exciton resonance, and in Figs. 4 and 5, and also in Figs. 6 and 7, the pump is detuned from the exciton resonance by $+\sqrt{2}\Gamma_0/2$ and $-\sqrt{2}\Gamma_0/2$, respectively. The abscissas on all plots are in dual energy units: on top are the more conventional meV units, and on the bottom are the FWHM units of $\sqrt{2}\Gamma_0$. We have chosen the FWHM units in order to give a measure of the relative strengths of the optical susceptibility and exciton absorption. The peak value of exciton absorption for all plots given here is $1.94 \times 10^4 \text{ cm}^{-1}$. Figures 2, 4, and 6 have values of $\gamma=0.1\Gamma_0$, while Figs. 3, 5,

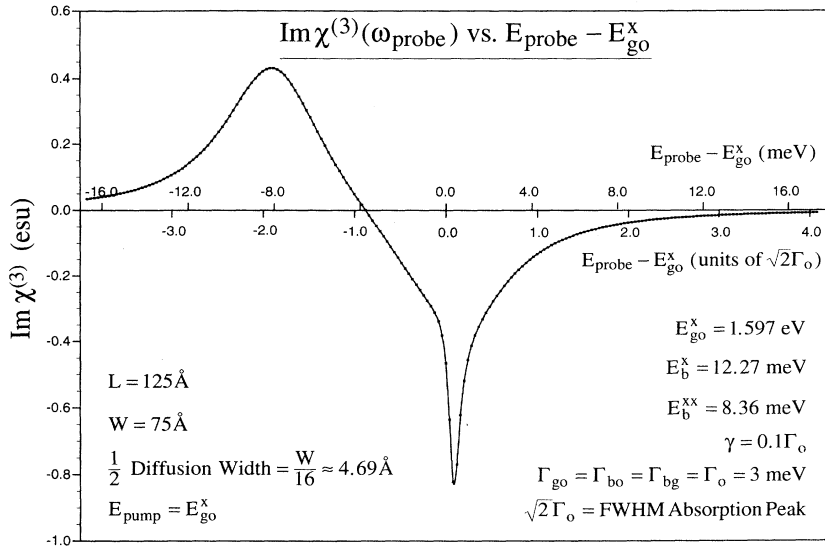


FIG. 2. The imaginary part of the third-order optical susceptibility as a function of the probe energy for a dual-beam pump-probe experiment. The pump is set at exciton resonance and the longitudinal broadening parameter is one-tenth the value of the transverse broadening parameters.

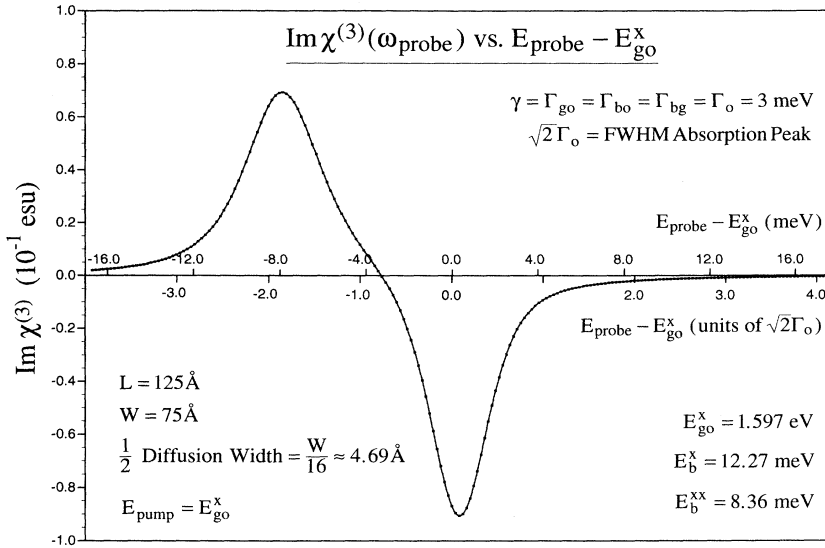


FIG. 3. Same as Fig. 2 but with the longitudinal broadening parameter equal to the transverse broadening parameters.

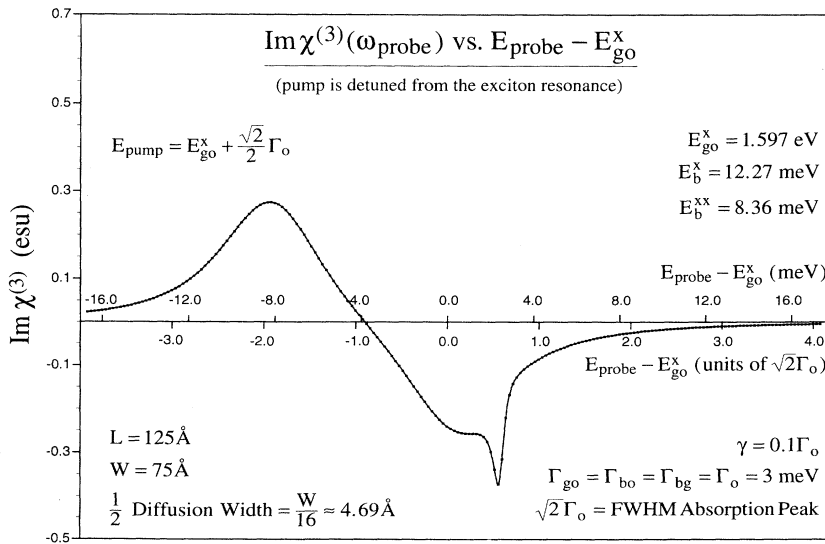


FIG. 4. Same as Fig. 2 but with the pump detuned slightly above the exciton resonance.

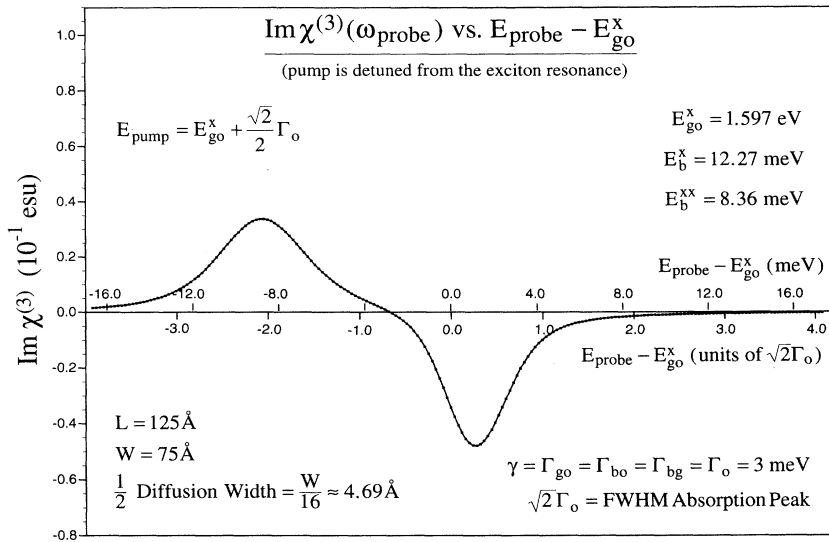


FIG. 5. Same as Fig. 4 but with the longitudinal broadening parameter equal to the transverse broadening parameters.

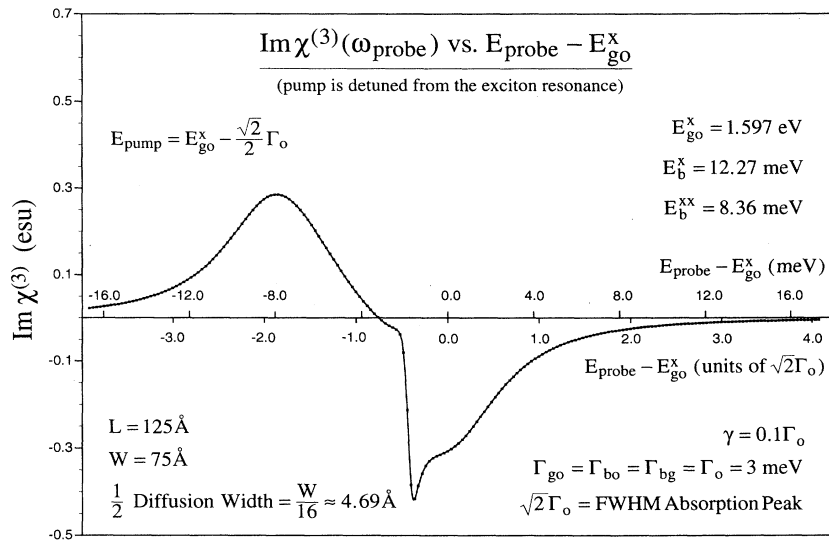


FIG. 6. Same as Fig. 4 but with the pump detuned slightly below the exciton resonance.

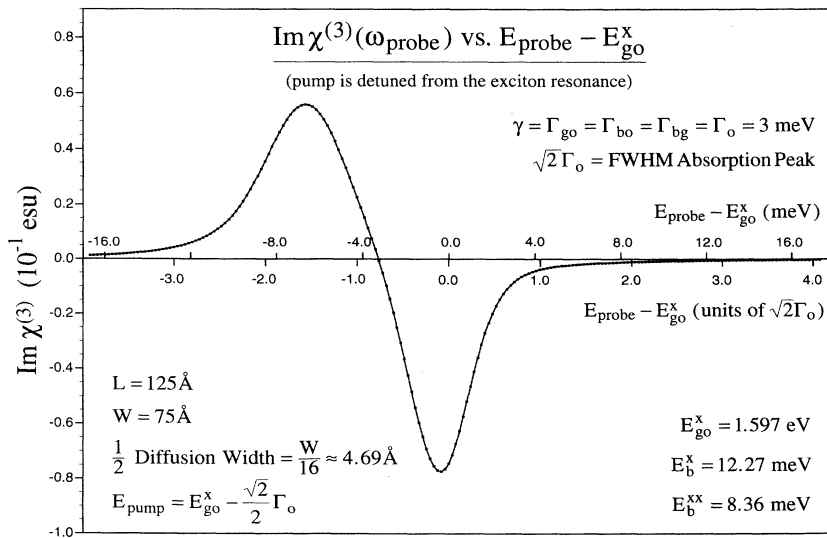


FIG. 7. Same as Fig. 6 but with the longitudinal broadening parameter equal to the transverse broadening parameters.

and 7 have values of $\gamma = \Gamma_{ij} = \Gamma_0$. Note that $-\text{Im}\chi^{(3)}$ is proportional to $-\Delta\alpha$, the differential change in optical transmission.

In comparing Figs. 2 with 3, 4 with 5, and 6 with 7, it is immediately apparent that Figs. 2, 4, and 6 all possess a rather abrupt, narrow negative peak for probe energies near or equal to the pump energies. The genesis of these peaks may be directly traced back to the $1/[\omega_r - \omega_2 + i\gamma]$ factor in Eq. (15) for the susceptibility. When $\chi^{(3)}$ is separated into real and imaginary parts, this factor leads to a resonance factor in both parts which goes as $1/[(\omega_r - \omega_2)^2 + \gamma^2]$. ω_2 corresponds to the pump, and the index r on ω_r is summed over values of 1 (probe) and 2. Since ω_1 is the probe, it is varied, and, when in resonance with ω_2 , the resonance factor becomes dominant [in the RWA the third line of Eq. (15) is negligible compared to the first two lines]. Its strength, however, is extremely sensitive to the magnitude of γ : when $\gamma = 0.1\Gamma_0$, its strength is 10^2 , or two orders of magnitude larger than when $\gamma = \Gamma_0$, as is the case in Figs. 3, 5, and 7. Physically, γ is related to the population decay rate of the exciton state. A smaller γ , then, means the lifetime of the exciton state is larger and that the exciton system is more stable. In turn, there is a higher probability of forming an excitonic molecule in a two-step photon absorption process. The resonance spiking is only significant if the detuning of the pump lies within 1–2 FWHM of the exciton absorption peak. Note that in Figs. 4 and 6 the curves tend to have a relative minimum at peak exciton absorption. Of course, when the pump is in resonance with the peak exciton absorption, the spiking is amplified even further, resulting in the curve displayed in Fig. 2. On the other hand, the curves displayed in Figs. 3, 5, and 7, those for which $\gamma = \Gamma_0$, show no sign of the abrupt spiking: the resonance factor is now approximately ten times smaller than before. The larger γ not only smears out the resonance spiking but it reduces the overall magnitude of each $\chi^{(3)}$ curve (note the scales of these curves are a factor of 10 times smaller).

The negative peak in all of these spectra, indicating transmission, is due to a bleaching (saturation) of the one-pair exciton transition. Physically, the initial exciton population created by the pump beam tends to amplify the probe beam, by way of stimulated emission, when the probe energy is tuned at or near the exciton linear absorption peak.

Another feature in all of the curves is the optical absorption—the region of positive $\text{Im}\chi^{(3)}$. The absorption may be attributed to the formation of the excitonic molecule.^{17–19} The initial exciton population enables the probe to be more strongly absorbed when its energy matches the exciton-biexciton transition energy $\hbar\omega_{g_0} - \hbar\omega_{bx}$. In the present case, the biexciton binding energy is 8.36 meV. The maximum of each curve occurs at energies slightly greater than $-2.0x\sqrt{2}\Gamma_0 = -9.3$ meV; in other words, very near the biexciton binding energy. Calculations for a wire of dimensions $L \times W = 225 \times 175 \text{ \AA}^2$ substantiate this interpretation. In that calculation, the biexciton binding energy was -5.55 meV, and the maxima of the $\text{Im}\chi^{(3)}$ curves occurred at energies slightly less than $-1.3 \times \sqrt{2}\Gamma_0 = -6.61$ meV.

In the last two plots, Figs. 8 and 9, we show typical curves for a single-beam pump-probe experiment, where $\gamma = 0.1\Gamma_0$ and Γ_0 , respectively. Since the pump and probe beams are always in resonance, the factor $1/[(\omega_r - \omega_2)^2 + \gamma^2]$ becomes just $1/\gamma^2$, which is constant, and it now acts to modulate the magnitude of $\text{Im}\chi^{(3)}$. Both curves exhibit a similar structure but, as expected, the curve for which $\gamma = 0.1\Gamma_0$ is approximately an order of magnitude larger.

IV. SUMMARY

We have solved the exciton/biexciton binding-energy problem in a three-parameter variational calculation in the effective-mass approximation for a rectangular GaAs quantum wire surrounded by $\text{Al}_{0.3}\text{Ga}_{0.7}\text{As}$ cladding material with finite Al graded band offsets included. For the

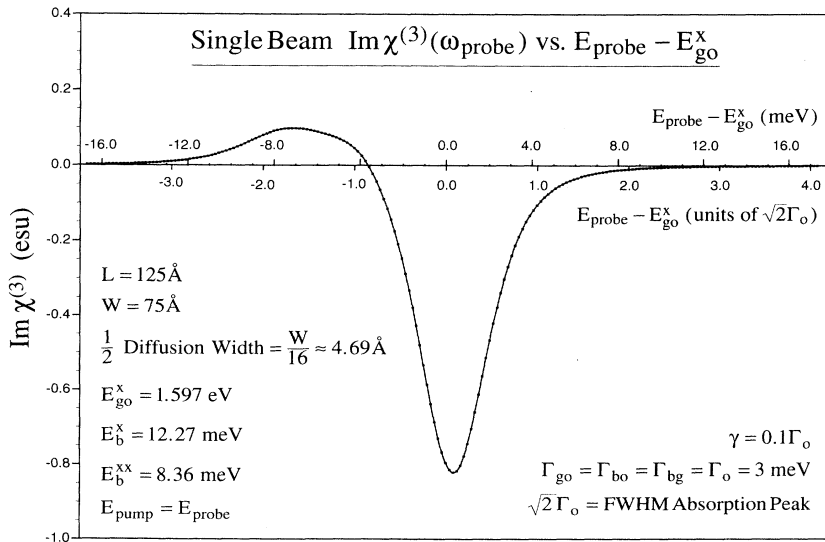


FIG. 8. The imaginary part of the third-order optical susceptibility as a function of the energy for a single beam pump-probe experiment. The longitudinal broadening parameter is one-tenth the value of the transverse broadening parameters.

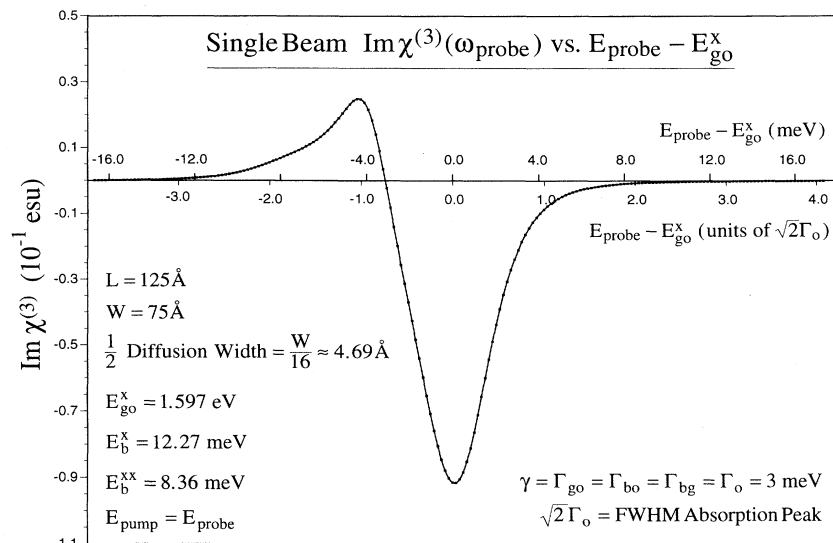


FIG. 9. Same as Fig. 8 but with the longitudinal broadening parameter equal to the transverse broadening parameters.

biexciton part of the problem, we employed a Heitler-London-type wave function.

Because of the inclusion of the graded finite band offsets, the single-particle states which make up the exciton/biexciton envelope functions had to be obtained numerically. For illustrative purposes we limited ourselves to one set of wire dimensions— $L \times W = 125 \times 75 \text{ \AA}^2$ —and four characteristic diffusion lengths $C = W/16$, $W/8$, $W/4$, and $W/2$. We then compared the single-particle and exciton-biexciton binding energies results with those of the previous calculation with infinite potential barriers by Madarasz and co-workers.¹⁴⁻¹⁶ All energies were lowered with the inclusion of the finite band offsets. For the narrowest grading, we found a percent difference of approximately 61% for the electron ground-state subband energy, while for the hole it was approximately 35%. The exciton and biexciton binding energies were both reduced by approximately 14%. As the grading widths increased, so did all energies, because as the diffusion width is increased the bottom of the well narrows, pushing the states up.

Next we applied the results of the exciton/biexciton calculation to obtain the nonlinear optical susceptibility $\chi^{(3)}$. Unlike our previous work,¹⁴⁻¹⁶ in which we calculated only peak values of $|\text{Im}\chi^{(3)}|$ for resonant exciton absorption using the RWA, here we studied $\text{Im}\chi^{(3)}$ as a function of pump-probe frequencies in a narrow range about the exciton resonant absorption. To do so, we used the general expression derived in the Appendix of our previous paper via a double Feynman diagram method.¹⁴ 16 diagrams all told. We then reasoned that near resonance the ground states of the exciton and biexciton would be the major contributors to $\chi^{(3)}$. Accordingly, we simplified the general expression, retaining only ground-state terms.

With the resulting expression, we calculated values for $\text{Im}\chi^{(3)}$ as a function of the pump and probe frequencies

for dual- and single-beam experiments. In each case, we repeated the calculation using two different sets of relaxation parameters: $\gamma = 0.1\Gamma_0$ and all $\Gamma_{ij} = \Gamma_0$; and for $\gamma = \Gamma_{ij} = \Gamma_0$. We found, in general, the structure of the $\text{Im}\chi^{(3)}$ curves to be strongly dependent on the values of relaxation parameters used. Specifically, in the present calculation, we found the overall magnitude and structure of the curves to be a strong function of the longitudinal relaxation parameter, γ . The smaller the value of γ , i.e., the longer the mean lifetime of the exciton, gave results which were systematically about an order of magnitude larger than when the larger value γ was used, and considerably enhanced the resonance when the probe equaled the pump in the dual-beam case, which was especially dramatic when the pump was slightly detuned from the exciton resonance. The maximum values of the resulting $|\text{Im}\chi^{(3)}|$'s were on the order of $10^{-2} - 10^{-1}$ esu.

A feature of all the curves was a region of positive $\text{Im}\chi^{(3)}$ for energies below the exciton saturation. The optical absorption was attributed to the biexciton formation. This absorption region was also of considerable magnitude but was displaced within 1–2 FWHM below the exciton resonance absorption, peaking at approximately the exciton-biexciton transition energy.

ACKNOWLEDGMENTS

The first author (F.L.M.) performed this research under AFOSR Contract No. F49620-J-0382. He is indebted to Dr. Patrick Hemenger of Wright Laboratory, Wright-Patterson Air Force Base, OH, and Lt. Col. Gernot Pomeranke of the Office Air Force Office of Scientific Research for their encouragement. The work of F.S. was performed under Air Force Contract No. F33615-91-C-5603.

- ¹S. Glutsch and F. Bechstedt, *Phys. Rev. B* **47**, 4315 (1993); **47**, 6385 (1993); *Superlatt. Microstruct.* **12**, 459 (1992).
- ²U. Bockelmann and G. Bastard, *Europhys. Lett.* **15**, 215 (1991).
- ³Mark Sweeny, Jingming Xu, and Michael Shur, *Superlatt. Microstruct.* **4**, 443 (1988).
- ⁴Ikuro Suemune and Larry A. Coldren, *IEEE J. Quantum Electron.* **QE-25**, 1778 (1988).
- ⁵Ladislav Bányai, Ian Galbraith, Claudia Ell, and Hartmut Haug, *Phys. Rev. B* **36**, 6099 (1987).
- ⁶K. Ishida and H. Aoki, in *Proceedings of the 21st International Conference on the Physics of Semiconductors, Beijing, China, 1992*, edited by Ping Jiang and Hou-Zhi Zheng (World Scientific Beijing, 1992), Vol. 1, pp. 213–216.
- ⁷Hiroaki Ando, Hironu Oohashi, and Hiroshi Kanbe, *J. Appl. Phys.* **70**, 7024 (1991).
- ⁸A. D'Andrea and R. Del Sole, *Phys. Rev. B* **46**, 2363 (1992).
- ⁹Eiichi Hanamura, *Phys. Rev. B* **37**, 1273 (1988); **38**, 1228 (1988); *Solid State Commun.* **73**, 551 (1990).
- ¹⁰R. Chen, D. L. Lin, and B. Mendoza, *Phys. Rev. B* **48**, 11 873 (1993). The results of this paper appear unphysical; the third-order susceptibility depends on the length of the wire.
- ¹¹D. A. B. Miller, D. S. Chemla, T. C. Damen, A. C. Gossard, E. Wiegmann, T. H. Wood, and C. A. Burrus, *Phys. Rev. B* **32**, 1043 (1985).
- ¹²D. S. Chemla, D. A. B. Miller, and S. Schmitt-Rink, in *Optical Nonlinearities and Instabilities in Semiconductors*, edited by Hartmut Haug (Academic, New York, 1988), pp. 38–120 and 325–359, and references therein.
- ¹³D. Gershoni, H. Temkin, G. J. Dolan, J. Dunsmuir, S. N. G. Chu, and M. B. Panish, *Appl. Phys. Lett.* **53**, 955 (1988).
- ¹⁴Frank L. Madarasz, Frank Szmulowicz, F. Kenneth Hopkins, and Donald L. Dorsey, *Phys. Rev. B* **49**, 13 528 (1994).
- ¹⁵Frank L. Madarasz, Frank Szmulowicz, F. Kenneth Hopkins, and Donald L. Dorsey, *J. Appl. Phys.* **75**, 639 (1994).
- ¹⁶Robert O. Klepfer, Frank L. Madarasz, and Frank Szmulowicz, *Phys. Rev. B* **51**, 4633 (1995).
- ¹⁷T. Takagahara, *Phys. Rev. B* **39**, 10 206 (1989).
- ¹⁸Y. Z. Hu, M. Lindberg, and S. W. Koch, *Phys. Rev. B* **42**, 1713 (1990).
- ¹⁹L. Belleguie and L. Bányai, *Phys. Rev. B* **47**, 4498 (1993).
- ²⁰L. Bányai, I. Galbraith, and H. Haug, *Phys. Rev. B* **38**, 3931 (1988).
- ²¹T. Ishihara, *Phys. Status Solidi* **159**, 371 (1990).
- ²²K. Brunner, G. Abstreiter, M. Walter, G. Böhm, and G. Tränkle, *Surf. Sci.* **267**, 218 (1992).
- ²³J. Boyd, H. Jackson, and A. Steckl (private communication).
- ²⁴Frank L. Madarasz and Frank Szmulowicz, *J. Appl. Phys.* **62**, 3267 (1987).
- ²⁵Hajime Ishihara and Kikuo Cho, *Phys. Rev. B* **42**, 1724 (1990).
- ²⁶T. Takagahara, *Solid State Commun.* **28**, 279 (1991).
- ²⁷H. Qiang, Fred. H. Pollack, C. M. Sotomayor Torres, W. Leitch, A. H. Kean, Michael A. Stroscio, Gerald Iafrate, and K. W. Kim, *Appl. Phys. Lett.* **61**, 1411 (1992).